Materials Today Advances 25 (2025) 100565

Contents lists available at ScienceDirect

Materials Today Advances

journal homepage: www.journals.elsevier.com/materials-today-advances/

Functionalization of chitosan with a polycarboxylic macrocycle yields injectable hydrogel with pH and salts responsiveness

Arthur Durand [a,b,1], Thomas Gréa [a,c,1], Gabin Lebeau [b], Guillaume Jacquot [d,e,f,g], Augustin Tillement [c,e], Axel Aigle [b], Eloïse Thomas [h], David Kryza [i,j], Jacqueline Taleb [i,k], Giuseppe Ferrauto [l], Eliana Gianolio [l], Alain Géloën [m], Alexandra Montembault [c], Maria Gutiérrez-Blanco [d,f,g], Xavier Pivot [d,f,g], Sébastien Harlepp [d,f,g], Alexandre Detappe [d,f,g], Laurent David [c,**], François Lux [a,n,*], Olivier Tillement [a]

[a] Institut Lumière Matière (ILM), Universite Claude Bernard Lyon 1, CNRS, UMR5306, F-69100, Villeurbanne, France
[b] MexBrain, 13 Avenue Albert Einstein, 69100 Villeurbanne, France
[c] Ingénierie des Matériaux Polymères (IMP), Universite Claude Bernard Lyon 1, INSA de Lyon, Universite Jean Monnet, CNRS, UMR 5223, Cedex, F-69622, Villeurbanne, France
[d] Institut de Cancérologie Strasbourg Europe, Strasbourg 67000, France
[e] Nano-H, Fontaines Saint Martin, France
[f] Strasbourg Drug Discovery and Development Institute (IMS), Strasbourg, 67000, France
[g] Equipe labellisée Ligue contre le Cancer, France
[h] Universite Claude Bernard Lyon 1, CNRS, Laboratoire d'Automatique de Génie des Procédés et de Génie Pharmaceutique (LAGEPP), UMR5007, Cedex, F-69622, Villeurbanne, France
[i] Imthernat Platform, Hospices Civils of Lyon, Lyon, 69003, France
[j] Service de Médecine Nucléaire LUMEN, Centre Léon Bérard, 15 Rue Gabriel Sarrazin, Lyon, 69008, France
[k] Gastroenterology and Technologies for Health, Centre de Recherche en Cancérologie de Lyon, INSERM U1052-CNRS5286, Universite Lyon 1, Lyon, 69008, France
[l] Molecular Imaging Center Department of Molecular Biotechnology and Health Sciences University of Turin, Turin, 10124, Italy
[m] Laboratoire Ecologie Microbienne (LEM), UMR CNRS 5557, INRAE 1418, Universite Claude Bernard Lyon 1, Domaine Scientifique de La Doua, Villeurbanne, 69100, France
[n] Institut Universitaire de France (IUF), Paris, 75005, France

ARTICLE INFO

Keywords:
Injectable hydrogel
Chitosan
DOTAGA
Drug delivery
Physical gelation

ABSTRACT

The development of injectable hydrogels that respond to physiological stimuli represents a promising strategy for a range of biomedical applications, although the precise tuning of gelation kinetics, mechanical stability, and biocompatibility remains a significant challenge. This study presents a pH- and osmolarity-responsive injectable hydrogel, formulated from a combination of chitosan and chitosan functionalized with a macrocyclic polycarboxylate. The functionalization of chitosan significantly modifies the electrostatic charges along the polymer backbone, enabling fast gelation under physiological conditions. The gelation process is driven by pH neutralization and osmolarity increase, where electrostatic interactions between the zwitterionic chitosan and unmodified chitosan generate a dynamic, entangled network strengthened by both electrostatic crosslinking and hydrophobic interactions. Rheological and structural analyses reveal the possibility of fine-tuning the gelation kinetics and mechanical properties by altering the ratio of zwitterionic chitosan to conventional chitosan in the formulation. Here, the optimized 67:33 % ratio achieved favorable compromise between rapid gelation and stability in physiological media. Different microscopy experiments, including conventional scanning electronic microscopy and live imaging, have confirmed the porous architecture of the hydrogels. *In vivo* experiments confirmed the injectability, biocompatibility, and biodegradability of the hydrogels, with gradual degradation observed by magnetic resonance imaging and fluorescence imaging over time in healthy mice after subcutaneous administration. Additionally, preclinical safety assessments in rabbits demonstrated good local tolerance to both single and repeated subcutaneous injections, with no systemic toxicity observed. These findings support the

* Corresponding author. Institut Lumière Matière, UMR5306, Claude Bernard Lyon1-CNRS University, University of Lyon, Cedex, 69622, Villeurbanne, France.
** Corresponding author.
E-mail addresses: laurent.david@univ-lyon1.fr (L. David), francois.lux@univ-lyon1.fr (F. Lux).
[1] Arthur Durand and Thomas Gréa contributed equally to this work.

https://doi.org/10.1016/j.mtadv.2025.100565
Received 15 November 2024; Received in revised form 27 January 2025; Accepted 29 January 2025
Available online 15 February 2025

potential for broad biomedical future applications, including drug delivery, wound healing, local metal uptake and tissue regeneration.

1. Introduction

Injectable hydrogels are materials that undergo a sol-gel transition at the administration site, enabling minimally invasive delivery offering and significantly reducing the risks associated with the implantation of conventional hydrogels such as infections, scarring and pain [1]. Hydrogels can be classified either into chemical hydrogels or physical hydrogels depending on the nature of their crosslinking. Chemical hydrogels are formed via covalent crosslinking between the polymer chains, often involving toxic reagents or ionizing radiations that may cause severe adverse effects [2] or require complex biodegradation strategies [3]. In contrast, physical hydrogels are generally safer and allow an easier *in situ* formation of the material [4]: crosslinking of the system is ensured by the formation of non-covalent bonds through the network. These bonds mainly include hydrogen bonds, electrostatic interactions, hydrophobic interactions, Van der Waals interactions or host-guest interactions and thus allow these systems to crosslink in response to external stimuli [5]. The growing interest in these injectable hydrogels has expanded their application as dermal filler, platform for drug delivery and materials for tissue engineering and regeneration. As of 2020, more than 30 injectable hydrogel formulations have received FDA and/or EMA approval, with many others in clinical trials [6–8]. Despite this progress, several challenges remain for the successful commercialization of injectable hydrogels. These include maintaining mechanical robustness post-formation while ensuring ease of injection, achieving rapid responsiveness in gelation upon administration, minimizing immunological reactions, and ensuring biodegradability [9].

Natural polymers are of great interest for developing injectable physical hydrogels due to their biocompatibility and biodegradability [10,11]. Chitosan in particular has been extensively studied in the development of hydrogels with applications in drug delivery [12], tissue reconstruction [13], wound healing [14] and dermal filling [15]. The physical gelation of chitosan-based materials can be triggered by several stimuli. Gelation of chitosan solutions can first occur thanks to a modification of pH using strong [16,17] or weak [18] bases: chitosan being soluble and cationic in acidic pH, the increase of pH above a critical chitosan concentration leads to a neutralization of the polymer resulting in a gelation. Thermosensitive chitosan hydrogels have also been developed, thanks to the presence of a weak base like β-glycerophosphate salt that enables gelation under heating [19]. Ionic crosslinking with anionic agents such as Guanosine 5'-Diphosphate (GDP) [20] or metals like molybdate [21] as well as the formation of polyelectrolyte complexes (PEC) between the cationic chitosan and an anionic biopolymer like alginate [22] or hyaluronate [23] are additional strategies for physical gelation. Solvent exchange, such as water evaporation from a hydroalcoholic solution of chitosan and washing also enables gelation [24]. However, many of these methods require harsh conditions (organic solvents, high pH) that make them hardly compatible with physiological environments. Recently, we introduced an innovative *in situ* gelling system using a chitosan functionalized with the macrocycle DOTAGA (chitosan@DOTAGA), mixed with unmodified chitosan for the subcutaneous (SC) delivery of monoclonal antibodies [25]. This system demonstrated controlled, adjustable, and extended antibody release compared to intravenous administration in both murine and non-human primate (NHP) models. In this study, we further investigate the physicochemical properties, the gelation mechanisms and microstructures of chitosan@DOTAGA mixtures, with a view to their use as a platform for drug delivery, tissue engineering, wound healing and local extraction of metals. Rheological analyses, morphology observations, and *in vivo* studies on different formulations were conducted to validate their biodegradability and their safety upon injection.

2. Results and discussion

2.1. Preparation and characterization of chitosan@DOTAGA

The elaboration of the injectable hydrogel formulation involves the synthesis of a derivative of chitosan, functionalized with DOTAGA. Prior to synthesis, the chitosan was fully characterized by ^{1}H NMR spectroscopy using the Hirai method [26] and yielded a degree of acetylation (DA) of 5.9 ± 0.3 % as published in the previous work [25]. The typical size characteristics and more precisely the number and weight average molar masses (M_n = 110 ± 3 kg/mol, M_w = 216 ± 3 kg/mol), the polydispersity and gyration radius of this starting chitosan were determined by High Performance Liquid Chromatography and Size Exclusion Chromatography coupled with refractive index and Multi-Angle Laser Light Scattering measurements (HPLC-SEC-MALLS) (Table 1) [27].

Functionalized chitosan@DOTAGA was prepared in a one-pot process where DOTAGA anhydride is directly added to a hydroalcoholic chitosan solution (Fig. 1A) [28,29]. The resulting product was purified by tangential filtration (cut-off: 100 kDa) followed by freeze drying. Unreacted remaining DOTAGA is quantified during the purification process by HPLC-SEC coupled with a UV detector (λ = 295 nm) to assess the purity (>95 %) of the resulting product. Chromatograms showed a shorter retention time for chitosan@DOTAGA than raw chitosan, highlighting the increase in molecular mass due to functionalization (Fig. 1C). The DA remained unchanged post-synthesis, and DOTAGA grafting was confirmed by Fourier-transform infrared spectroscopy (FT-IR) (Fig. S1). The Degree of Substitution (DS) corresponding to the grafting degree of DOTAGA on the chitosan backbone was estimated at 17.1 ± 0.5 % using copper (Cu^{2+}) dosage (Fig. 1B). Number and weight average molar masses, polydispersity and gyration radius of this resulting functionalized chitosan have also been determined (Table 1). The experimentally observed mass increase in M_n and M_w matched the theoretical increase by a factor of 1.49, consistent with the degree of DOTAGA substitution. Chitosan@DOTAGA chains conformations at 0.1 w/w % exhibit a significative smaller gyration radius than raw chitosan (in acetate buffer, pH = 4.8) which can be easily ascribed to the presence of electrostatic interactions between the negatively charged DOTAGA and positively charged protonated amino groups of glucosamine units resulting in a more compact chains conformation than raw chitosan which presents an extended polyelectrolyte conformation due to the repulsive interactions between its protonated amine functions.

2.2. Solubility properties of the zwitterionic chitosan@DOTAGA, chitosan and their mixes

The modification of chitosan backbone with DOTAGA drastically changes some of its physicochemical properties due to steric hindrance and the introduction of negative charges from the macrocyclic group. Chitosan, a polycationic polymer, is soluble in mild acid conditions via protonation of its amine groups (pKa = 6.2 for DA = 0 %) but becomes insoluble at physiological pH due to the neutralization of electrostatic repulsive forces [27]. DOTAGA being a macrocyclic molecule composed of four amine moieties and four carboxylic groups has a versatility of charges according to the pH (protonation constant associated to DOTAGA, COOH: pKa_1 = 1.71, pKa_2 = 1.88, pKa_3 = 4.18, pKa_4 = 4.24. NH^+: pKa_1 = 9.23, pKa_2 = 11.08) [30]. From pH = 4.2 to pH = 6.9, the DOTAGA graft thus possesses a global negative charge due to the dissociation of carboxylic groups, while the amine groups of the glucosamine units are still partially protonated. This imparts a

polyampholytic character of the whole chain, chitosan@DOTAGA being zwitterionic (neutral) at its isoelectric point at a pH of 6.9 [25]. At basic pH, only DOTAGA should retain a negative charge, imparting a polyanionic nature and increased hydrophilicity to chitosan@DOTAGA compared to ungrafted chitosan (Fig. 2A).

The chemical modification induced by DOTAGA grafting thus led to a distinct solubility behavior of the polymer (Fig. 2B). At a concentration of 1 % w/w, ungrafted chitosan remains soluble in an acidic environment until a pH of 6.5 is reached consistently with the apparent pKa of amine groups [27]. The impact of NaCl concentration on the solubility of chitosans of different DAs and at different concentrations in acidic aqueous solutions was previously investigated [31]. Chitosan of DĀ6 % at a concentration of 1 % typically precipitates at a NaCl concentration above 0.5 mol/L (*i.e.* >1 osm/L), well above the osmolarity range investigated here, up to physiological values. In contrast, the solubility properties of chitosan@DOTAGA are more strongly impacted by the presence of salt, which causes it to become less soluble in acidic saline solutions as the osmolarity increases. Additionally, above a pH of 7, chitosan@DOTAGA becomes soluble again in basic media, possibly due to the polyanionic nature of the grafted chains in this pH range, regardless of the osmolarity. Mixed Chitosan@DOTAGA:Chitosan formulations (50:50 % and 67:33 %) were also examined, both inheriting the osmolarity sensitivity of chitosan@DOTAGA in acidic media and the insolubility of ungrafted chitosan at neutral and basic pH, thereby ensuring gel stability under physiological conditions.

2.3. Formulation of chitosan@DOTAGA:Chitosan mixture and associated gelation mechanisms and kinetics

2.3.1. Rheological properties of solutions

Three formulations, with chitosan@DOTAGA:chitosan ratios of 100:0 %, 67:33 % and 50:50 % were prepared at pH ≈ 5.5 and a total polymer concentration of 5 % w/w by dissolving raw chitosan and chitosan@DOTAGA in an acetic acid solution. After solubilization via mechanical stirring and steam sterilization of the mixture, the Newtonian viscosity of each solution was measured on a rheometer equipped with a cone-plane geometry (Fig. 3A). Detailed flow diagrams combining the viscosity measured by a cone-plane rheometer and an injection system assimilated to a capillary rheometer are also provided in the supplementary data section (Fig. S2). The injectability of the formulations was assessed by measuring the ejection force required to extrude the material through a 25 G x 16 mm needle at an injection rate of 1 mm/s (Fig. 3A). As deduced from injectability tests, all formulations possess an appropriate viscosity at room temperature to allow feasible injection through a 25 G needle. Formulations with higher chitosan@DOTAGA:chistosan ratio showed lower viscosities, likely due to the more compact chain conformations (see Table 1 for the values of gyration radius of chitosan and chitosan@DOTAGA) resulting from intermolecular ionic interactions in chitosan@DOTAGA, which reduce entanglement density.

2.3.2. Gelation kinetics and rheological properties

After characterization of solution rheological properties, we evaluated the gelation kinetics of the resulting hydrogels after immersion in PBS (pH = 7.4, osmolarity = 300 mOsm/L), to assess the impact of chitosan@DOTAGA (Fig. 3B). The 100:0 % chitosan@DOTAGA:chitosan formulation has a rapid sol-gel transition in PBS medium but gradually re-solubilizes after 2 h already, losing over 50 % of its mass after 24 h. This behaviour is likely attributable to the proximity of the chitosan@DOTAGA solubility domain (at pH = 7.5, see Fig. 2B) and the specific role of phosphate ions, interacting with chitosan backbone segments [32] in competition with hydrophobic interchain interactions. On the other hand, the 0:100 % chitosan homopolymer did not gel spontaneously in PBS and the 50:50 % chitosan@DOTAGA:chitosan formulation tended to gel slowly, forming a very soft hydrogel after 24 h. Incorporating a higher fraction of chitosan@DOTAGA (67:33 %) resulted in a more favorable balance, with gelation occurring within 2 h of immersion in PBS. This faster gelation could be driven by increased osmolarity, enhanced chain flexibility, and electrostatic interactions between the DOTAGA-modified and unmodified chitosan components. Over time, this initial gel evolved into a more rigid and stable structure, likely due to neutralization effects, the formation of hydrophobic interactions, and crystallization of the chitosan backbone segments. The rheological profile of the 67:33 % formulation supports its suitability for subcutaneous administration, as it exhibits injectability, *in situ* gelation upon contact with physiological fluids, and sufficient cohesiveness to prevent diffusion into surrounding tissues. Moreover, it demonstrated resilience against the mechanical stresses typical of the subcutaneous environment [33]. The various electrostatic interactions of the grafted polymer help to preserve a density of entanglement nodes during the neutralization of the system which allow a sol-gel transition by the formation of a tightly interconnected network by physical crosslinking in response to the neutralization of the pH. This electrostatically driven gelation was further validated by pre-complexing 70 % of the DOTAGA groups with gadolinium ions (Gd^{3+}) before pH neutralization, which prevented precipitation, confirming the importance of these interactions. Going forward, Gd^{3+}-complexed formulations will be utilized to assess biodegradability, with gadolinium concentrations restricted to 300 ppm.

To sum up the observations made in the previous sections, chitosan@DOTAGA:chitosan mixed solutions at pH = 5.5 and at total polymer mass concentration of 5 % form a dynamic entangled network where electrostatic interactions and polyelectrolyte complexes stay limited, at low ionic force, by the rigidity of the polycationic chitosan backbone: the rigidity of the polyelectrolyte chains is strong enough to limit the formation of dense polyelectrolyte complexes involving the negatively charged DOTAGA groups interacting with possibly several protonated amine groups, since the viscosity of the solution decreases with added chitosan@DOTAGA. When the formulation is immersed in a medium representative of physiological pH (7.4) and physiological osmolarity (300 mOsm/L), the diffusion of the buffer ions induces partial electrostatic screening and ensures a greater flexibility of the polyelectrolyte backbones, which then allow to form more polyelectrolyte complexes and then a first polyelectrolyte gel. Subsequently, the amine groups are progressively neutralized, causing the gelation and crystallization of chitosan backbone segments. Previous polyelectrolyte interactions may be stabilized by the establishment of weaker (hydrogen) bonds [34] after neutralization of amine groups. The system thus maintains an entangled state thanks to the existence of these successive interactions until the system is completely set by complete gelation of

Table 1
Detailed macromolecular structure characterization of initial chitosan and chitosan@DOTAGA derivative.

Product	Acetylation Degree [%]	Substitution Degree[a] [%]	Cu Uptake Capacity[b] [mg/g]	Molar Masses [kg/mol]		Polydispersity	Gyration Radius [nm]
				M_n	M_w	M_w/M_n	$R_{g,w}$
Chitosan	5.9 ± 0.3	0	N/A	110 ± 3	216 ± 3	1.96 ± 0.05	46 ± 2
Chitosan@DOTAGA	5.9 ± 0.3	17.1 ± 0.5	45 ± 1	153 ± 2	316 ± 3	2.06 ± 0.03	31 ± 2

[a] Deduced from expected chemical structure as displayed in Fig. 1A
[b] 1 g/L polymer solution in 0.1 mol/L acetate buffer solution (pH = 4.5) copper dosage with $[Cu^{2+}] \in [0,1]$ mmol/L.

the chitosan backbone chains, leading to a semi-crystalline hydrogel [35].

2.3.3. Microstructural analysis of hydrogels

Small-Angle synchrotron-X-ray Scattering (SAXS) analyses were performed on gels formed at 5 % w/w in a phosphate buffer at pH = 7.4 with an osmolarity of 300 mOsm/L. We analyzed the neutralized systems prepared with initial non-grafted chitosan 0:100 %, chitosan@DOTAGA 100:0 % and a 67:33 % chitosan@DOTAGA:chitosan mixtures to study the microstructure at the nanoscale (Fig. 3C). For raw chitosan hydrogel, the scattered intensity pattern ($I(q) \sim q^{-4}$ at $q > 2.5 \times 10^{-2}$ Å^{-1}; where $q = 4\pi sin(\theta)/\lambda$) is typically associated with a structure where two phases are separated by a rather sharp interface possibly resulting from the amorphous and crystalline phases [36]. In the lower q-range, the Guinier law can be applied $I(q) = I_0 \exp(-R_{g,c}^2/3\ q^2)$, where $R_{g,c}$ (~120 Å) is the mean gyration radius of crystallites (Fig. S3). In the q-range $q < 8 \times 10^{-3}$ Å^{-1}, the upturn in scattered intensity reveals larger scale heterogeneities (micron range pores or clusters) [37]. The scattering diagram of chitosan@DOTAGA hydrogel appeared quite different with absence of any clear Guinier regime in the investigated q-range, possibly associated to a more homogeneous structure at the nanoscale. However, in the q-range where $q > 3 \times 10^{-2}$ Å^{-1}, the scattered intensity scales as $I(q) \sim q^{-1}$ possibly associated with a rod-shaped chain portion [38]. At very low q however, the intensity gradually increases, which can reveal the presence of micron-range aggregates/voids within the hydrogel structure. Finally, the pattern of the SAXS profile resulting from the 67:33 % hydrogel is found intermediate between the scattering patterns of each of the two homopolymer gels, thus with intermediate scaling exponent ($I(q) \sim q^{-2}$).

Wide-Angle X-ray Scattering (WAXS) analyses have also been performed simultaneously for the same formulations at the same pH as SAXS but this time for hydrogels formed in Phosphate Buffered Saline (PBS) solution at 10 mmol/L to evidence the formation of chitosan crystallites (Fig. 3D). The WAXS profile of unmodified chitosan solution neutralized in PBS displays a main halo due to the presence of water with broad maximum close to 2 Å^{-1}, and a crystallinity peak at 1.36 Å^{-1} which can be compared to the *200* reflection for the hydrated chitosan allomorph [39], expected close to $q = 1.42$ Å^{-1}. This peak is also present on the WAXS profile of the 67:33 % ratio hydrogel, but cannot be seen for chitosan@DOTAGA alone. The ratio of the peaks areas between 67:33 % system to raw chitosan 0:100 % is close to 27 % which indicates that the crystallinity of hydrogels is proportional to the fraction of unmodified chitosan and that no co-crystallization between chitosan and chitosan@DOTAGA occurred. This finding can further be confirmed by the apparent crystallite size deduced from the Scherrer equation, which appears to be the same for 0:100 % chitosan homopolymer hydrogel and a 67:33 % mixture, and was estimated to be around 230 Å. This value corresponds to twice the value of the radius of gyration and seems to coincide with the SAXS analysis (Fig. S3).

When the hydrogels were formed in faster neutralization conditions by immersion in a 3M NaOH aqueous solution, both raw chitosan and 67:33 % formulations exhibited crystallinity (Fig. S4). In this case, the area of *200* reflection peak of the 67:33 % hydrogel was only 15 % of that of ungrafted chitosan hydrogel. In such fast neutralization and gelation conditions, disentanglements between chitosan@DOTAGA and chitosan are less effective and non-crystallizable chitosan@DOTAGA may significantly hinder chitosan crystallization. However, neutralization in PBS may be a slower process giving time for chitosan@DOTAGA and chitosan chains to disentangle, thus favouring chitosan separate crystallization. This is further confirmed by a smaller Scherrer crystallite

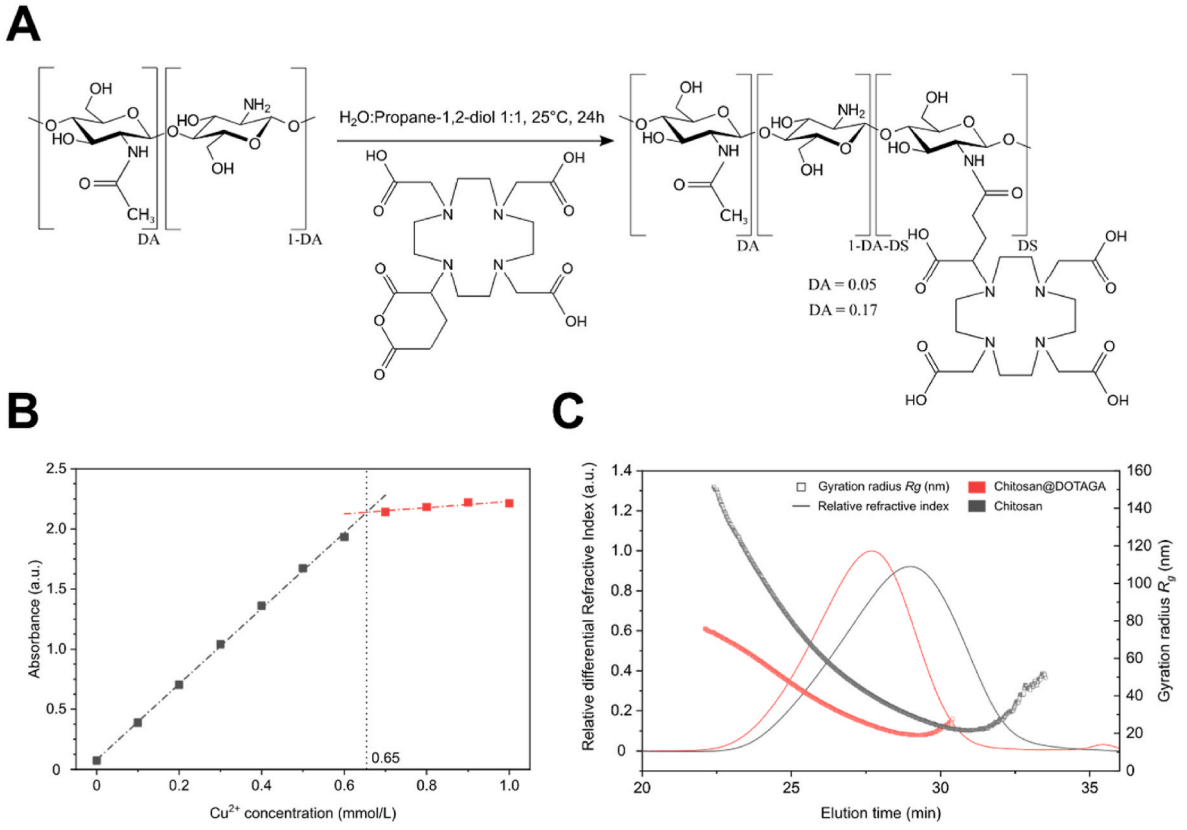

Fig. 1. Chitosan@DOTAGA synthesis and determination of its structural properties. **A)** Simplified reaction scheme for chitosan@DOTAGA synthesis, **B)** Determination of the degree of substitution (DS) of DOTAGA grafted on chitosan by copper dosage revealing a copper uptake capacity of 45 ± 1 mg/g corresponding to a DS = 17.1 ± 0.5 %, **C)** HPLC-SEC-MALLS chromatograms and gyration radius $R_{g,w}$ of both of DOTAGA-functionalized and unmodified chitosans as a function of polymer elution time.

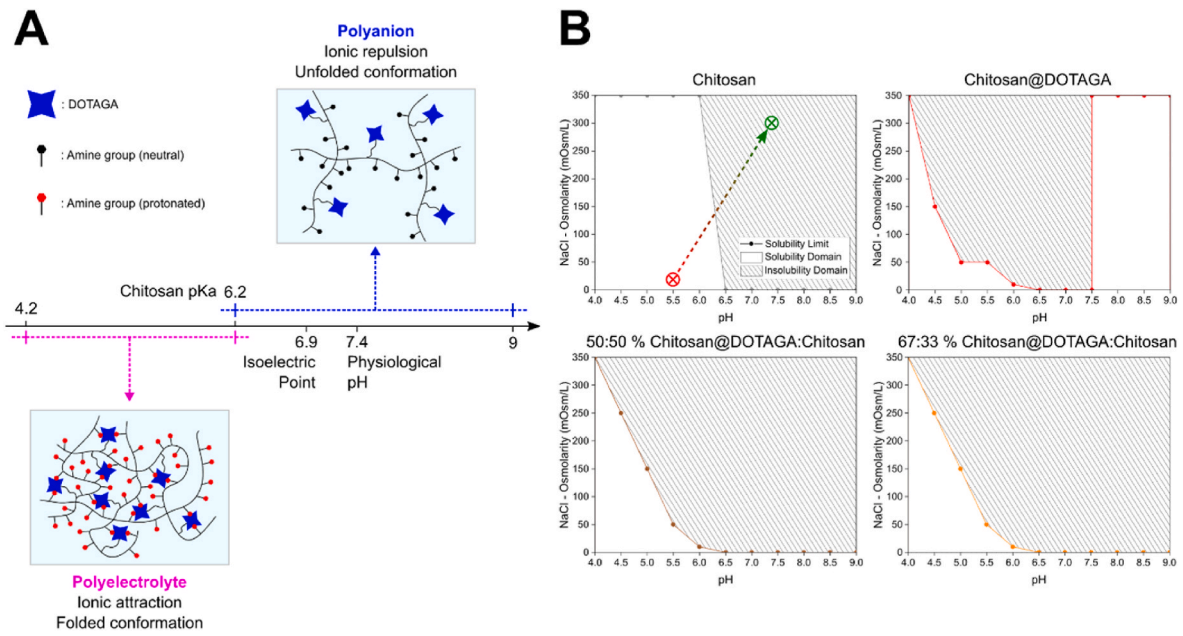

Fig. 2. A) Conformations of chitosan@DOTAGA and predominance diagram of acid-base forms of chitosan@DOTAGA showing a versatility of electrostatic charges as a function of pH with an isoelectric point centred around neutrality, **B)** Solubility diagram of different polymer systems at a concentration of 1 w/w % with pH and osmolarity. Osmolarity was controlled by NaCl addition. Grafting DOTAGA induces solubility at high pH, but reduces solubility at acidic pH due to DOTAGA/amine electrostatic interactions. Chitosan@DOTAGA/chitosan mixes retain the solubility domain common to both polymers with only slight variations with composition of the mixes. The trajectory shown on the solubility diagram of chitosan displays the evolution of pH after injection of a solution *in vivo,* in contact with body fluids. Such trajectory induces gelation of chitosan@DOTAGA/chitosan formulations sooner due to their sensitivity to osmolarity.

size of around 110 Å for both chitosan and 67:33 % mix hydrogels formed in 3 mol/L sodium hydroxide bath. FT-IR analysis of the chitosan@DOTAGA:chitosan 67:33 % lyophilized hydrogel (Fig. S5) revealed an intermediate profile between the two of the polymers alone (Fig. S1) without any additional peak, confirming the physical nature of the crosslinks.

2.3.4. *Hydrogel microscopic morphological appearance*

In order to evaluate the impact of the chitosan@DOTAGA content for a given formulation on the resulting structure of the hydrogel, Scanning Electron Microscopy (SEM) was carried out on hydrogels of three different formulations. Alcogels were formed by successive immersions of the hydrogels in ethanol:H_2O solutions with increasing ethanol concentrations before being dehydrated by CPD with supercritical CO_2. The gels formed from the 67:33 % and 50:50 % ratios both exhibited a fine structure with a tightly interconnected network and micron-sized pores. The gel resulting from the 67:33 % formulation presents a more pronounced porosity with a microscopic web-like arrangement (Fig. 4A) while the gel from the 50:50 % formulation (Fig. S6A) presents a structure with slight clusters reminiscent of a classic raw chitosan hydrogel structure [37]. The formulation composed only of chitosan@DOTAGA presented a very smooth surface without a clear porous structure (Fig. S6C): this may be due to an alteration of the hydrogel morphology during solvent exchange or dehydration process resulting in an image that does not seem representative of the hydrogel native morphology.

Supercritical CO_2 drying has been demonstrated to better preserve the original nanostructure of alginate hydrogels compared to lyophilisation [40,41]. However, this property may change for chitosan, hence it was necessary to verify if the porous structure evidenced by SEM was effectively representative of the micron-range microstructure of native hydrogels in presence of water. In this context, we were able to image chitosan@DOTAGA:chitosan hydrogels using a refractive index (RI) microscope (3D live cell imager). Indeed, holotomographic microscopy has recently shown great potential for imaging hydrogels [42]. Three formulations were imaged in 3D across multiple planes using this technique (Fig. S7A-C), allowing the visualization of the internal structure of the hydrogels without the influence of dehydration artifacts. The resulting images were analyzed by calculating monodimensional autocorrelation functions, which provided quantitative insights into the spatial organization and periodicity of the hydrogel network. Fig. 4B displays *Oxy* plane RI images of chitosan@DOTAGA:chitosan 100:0 % at 5 % w/w, chitosan@DOTAGA:chitosan 67:33 % at 5 % w/w and chitosan@DOTAGA:chitosan 67:33 % at 2.5 % w/w). Hydrogels containing only chitosan@DOTAGA exhibit a weblike structure characterized by alternating zones of low polymer concentration ("pores") with an average size of around 6 μm and polymer rich-zones with high RI (~1.5 μm). On the other hand, chitosan@DOTAGA:chitosan 67:33 % at 5 % w/w formulation appears to result from aggregated, tightly-packed spheres, revealing smaller pore sizes (~1 μm) and larger entangled polymer-rich zones consistent with the increased viscosity previously observed in the rheological studies. Such structural differences could result from the different scenarios of gelation: the fast polyelectrolyte complex formation of chitosan@DOTAGA yields a fibrillar nanostructure (possibly similarly to calcium alginate hydrogels [40]). The 67:33 % formulation containing non-grafted chitosan, however, undergoes slower gelation, promoting chitosan crystallization into larger clusters [37]. For the 67:33 % formulation at 2.5 % w/w, a similar microstructure to the 5 % w/w formulation was observed, albeit with pore sizes approximately five times larger. This highlights the impact of polymer concentration on pore formation and network organization within the hydrogel. In all, refractive index microscopy revealed structures with similar dimensions that those observed in SEM, with a possibility to observe native hydrogels and to extract more precise figures about the distribution of matter and pores in these systems. These observations showed that the chitosan@DOTAGA-based hydrogels display a porous structure that can be controlled by modification of either the chitosan@DOTAGA:chitosan ratios or the total polymer concentration, making this system highly adaptable for optimizing drug delivery profiles and controlling hydrogel biodegradation rates [12]. These aspects, including biocompatibility and biodegradation, are further explored in the following section.

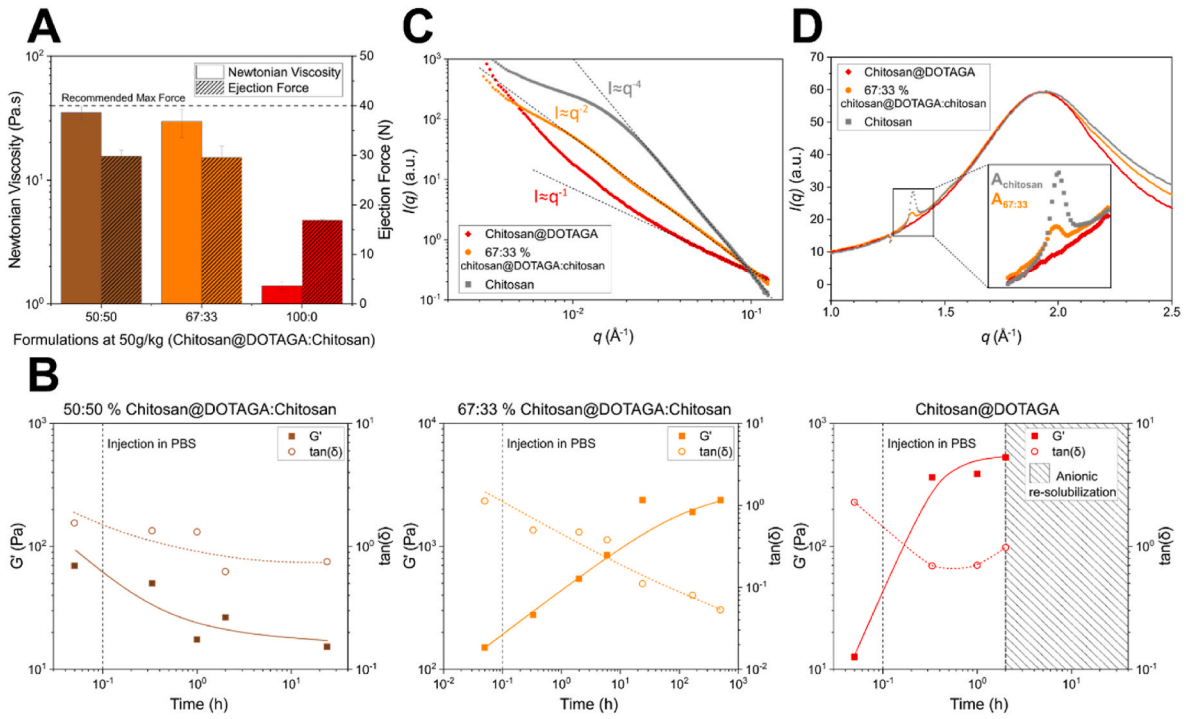

Fig. 3. Determination of rheological properties and associated nanoscale structural properties of different chitosan@DOTAGA:chitosan formulations. **A)** Newtonian viscosity of formulations at 5 w/w % (pH = 5.5) deduced from the flow diagram ($\eta = f(\dot{\gamma})$) at low shear rates $\dot{\gamma}$. A decrease in viscosity with chitosan@DOTAGA mass fraction is evidenced by rheology measurements. Ejection forces (N) required to inject different formulations through a 16 mm long 25 G needle in a 1 mL BD Hylok™ glass pre-fillable syringe at a plunger speed of 1 mm/s highlighting the feasible injectability of all systems by a practitioner and the increase of viscosity with chitosan@DOTAGA loading, **C)** SAXS analyses performed on different formulations previously immersed in a phosphate buffer and revealing their nanoscale structural properties with Porod's law $I(q) \sim C/q^4$ exhibited by semicrystalline chitosan hydrogel, $I(q) \sim C/q$ displayed by (non-crystalline) ampholyte chitosan@DOTAGA solution and intermediate scattering regimes of the 67:33 % mixed formulation, **D)** WAXS study of hydrogels formed after immersion of solutions in PBS (10 mmol/L) for different formulations, evidencing crystallinity induced by gelation of raw chitosan with *(200)* diffraction reflection of anhydrous allomorph. The main halo is due to water. **B)** Oscillatory rheological properties (ω = 10 rad/s, strain of 1 %, 25 °C) of hydrogels obtained from different formulations at total chitosan concentration of 5 w/w %, at different times in PBS (10 mmol/L) revealing better mechanical properties and a higher gelation kinetics for the 67:33 % formulation. The 100:0 % formulation exhibits a fast gelation kinetics, but starts to redissolve after 2 h immersion in PBS.

2.4. Pre-clinical validation of the designed injectable hydrogel

2.4.1. In vivo biodegradability and bio-elimination in vivo

Preclinical studies were conducted to assess the applicability of these hydrogel formulations for biomedical applications requiring various rates of resorption. For this experiment, chitosan@DOTAGA labelled with cyanine 5.5 by chemical grafting and chitosan@DOTAGA marked with gadolinium (III) by complexation of about 70 % of its DOTAGA were added to a mixture of non-labelled polymers to evaluate the *in vivo* biodegradation of the hydrogels as well as their biodistribution after injection. A total of 150 µL of pre-labelled 67:33 % and % 100:0 % formulations were subcutaneously administered in the neck of nude mice for each formulation studied (n = 3/group).

The two primary formulations exhibited similar rates of degradation over the first 17 days post-administration, with a reduction in fluorescence intensity of more than 60 % during this period (Fig. 5A–C). Similarly, the mean fluorescence area decreased significantly, with a reduction in the surface occupied by the gel across both formulations (Fig. 5D). As expected, the 67:33 % formulation having a higher viscosity and gelation capacity resulted in a more localized injection, with the gel remaining concentrated near the injection site. In contrast, the 100:0 % formulation which is only composed of chitosan@DOTAGA spread more significantly to the surrounding tissues. This dispersal is consistent with the rheological data, where the 100:0 % system was found to be unstable in PBS and redissolved within 2 h (see Fig. 3B). By day 21, the mice injected with the 67:33 % formulation macroscopically still showed minimal traces of gel at the injection site, reflecting incomplete degradation over 3 weeks, unlike the 100:0 % formulation. Bio-elimination through renal clearance was confirmed by collecting organs of each mouse and performing Inductively Coupled Plasma Mass Spectrometer (ICP-MS) measurement of gadolinium (Fig. 5B), which is consistent with clearance pathways already reported for chitosans [43]. No significant bioaccumulation of gadolinium was observed in any organs. A third formulation, with chitosan@DOTAGA:chitosan ratio of 83:17 % was also evaluated *in vivo* and demonstrated an intermediate degradation profile between the 100:0 % and 67:33 % formulations (Fig. S8).

Given the rheological and microstructural results which demonstrated that the 50:50 % and 100:0 % formulations do not result in stable hydrogels, we focused only on the 67:33 % formulation. The subcutaneous biodegradation of this formulation was further assessed using MRI, employing Gd^{3+}-precomplexed chitosan@DOTAGA as a contrast agent (Fig. 6A) to estimate whether complete degradation of the hydrogel could occur over a longer period after injection. Hence, post-injection MRI monitoring of the formulation shows a significant decrease in the volume occupied by the hydrogel over time. By day 30 post-injection, the volume occupied by the implanted hydrogel decreased by approximately 50 %, accompanied by a sixfold increase in the T_1 value within the same area, indicative of the gradual dissipation of gadolinium at the administration site (Fig. 6B). Interestingly, from day 4 onward, T_2-weighted began to show heterogeneity in the region of interest (Fig. S9), indicating cellular infiltration into the hydrogel structure. By day 15, this heterogeneity became more pronounced, as observed in the increasing standard deviations of the T_1 values measured up to day 28. Additionally, histological analysis confirmed these findings revealing a heterogeneous structure composed of compact zones

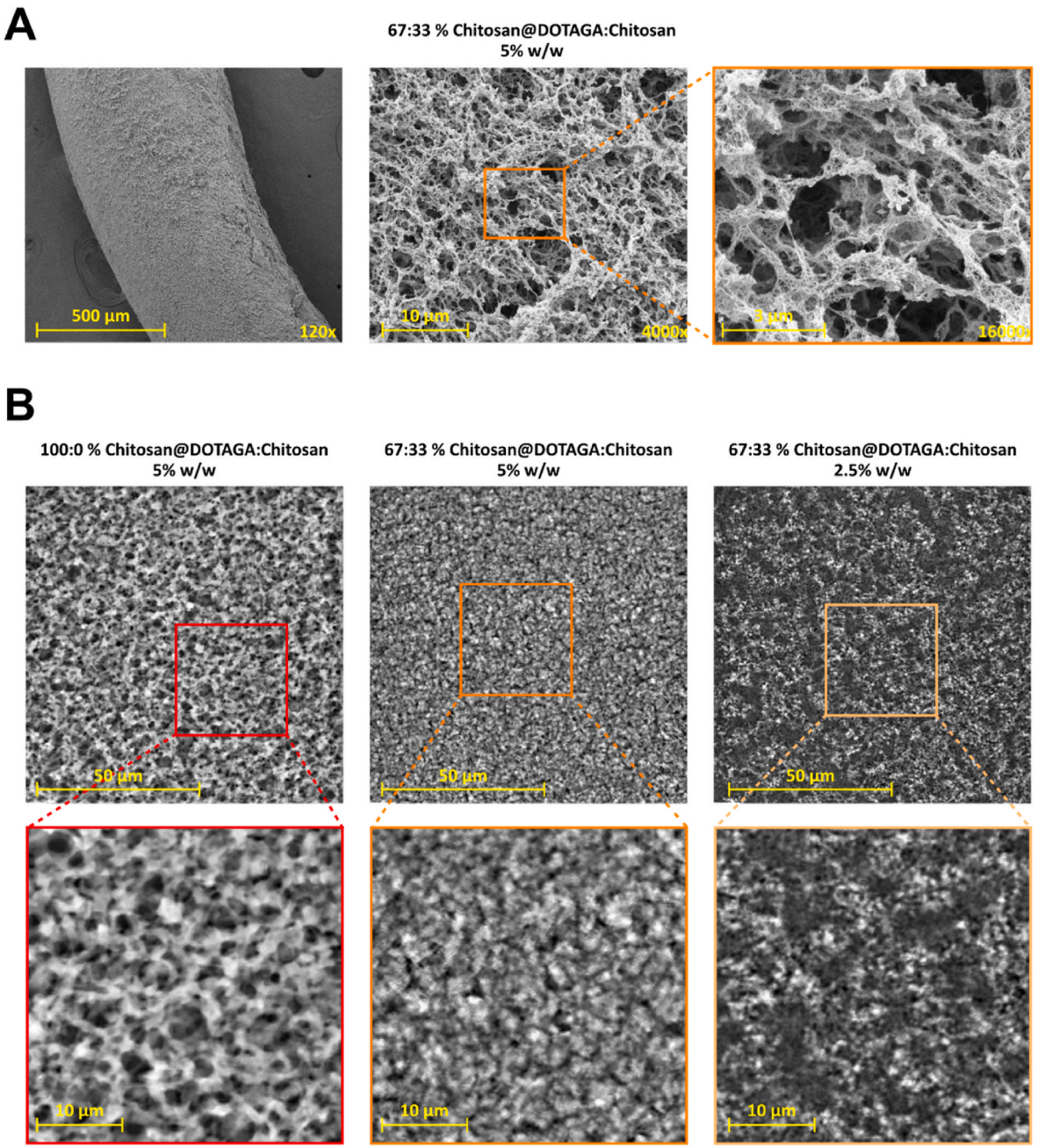

Fig. 4. A) SEM micrographs of the morphology of chitosan@DOTAGA:chitosan 67:33 % at 5 % w/w formulation obtained on hydrogel dried by critical point drying method with supercritical CO_2 at different magnifications highlighting the porosity network obtained for this formulation, **B)** 3D live cell imager Refraction Index microscopy images of different hydrogel formulations (without drying) of chitosan@DOTAGA:chitosan mixtures at different magnifications, namely: chitosan@DOTAGA:chitosan 100:0 % 5 % w/w, chitosan@DOTAGA:chitosan 67:33 % 5 % w/w, and chitosan@DOTAGA:chitosan 67:33 % 2.5 % w/w.

with gel fragments and less dense regions with visible cellular infiltration at high magnification (Fig. 6C). The degradation profile observed in the longitudinal MRI study aligns with the fluorescence imaging, indicating a rapid degradation phase in the first days post-administration. While a 50 % decrease in volume was recorded at the end of the 28-day study, this value likely underestimates the true degradation due to the contribution of cellular infiltration, which progressively increased the measured volume.

2.4.2. *Biosafety and local tolerance of SC administration*

The local tolerance to the 67:33 % formulation was evaluated after a single or repeated subcutaneous administrations of 500 µL/site of the formulation to female New Zealand White rabbits (Fig. 7A). The study was performed under good laboratory practice (GLP) using 4 groups, each of 3 female animals. Groups 1, 2 and 3 were dosed once on Day 1 and were sacrificed on Day 22 (Week 4), 43 (Week 7) and 64 (Week 10) of the study, respectively. Group 4 was dosed on Days 1, 22, 43 and 64 in 4 different sites in the scapular region and was sacrificed on Day 71 (Week 11) (Fig. 7B).

No mortality or adverse clinical signs, including erythema or edema, were observed in any animals throughout the study period, and body weight remained unaffected by the treatment with the injectable hydrogel formulation (Fig. 7D). Microscopic examination across all four groups revealed no substantial differences and consistently showed granulomatous inflammation (foreign body reaction) localized in the dermis and subcutis at the injection site. Histological analysis (Fig. 7C)

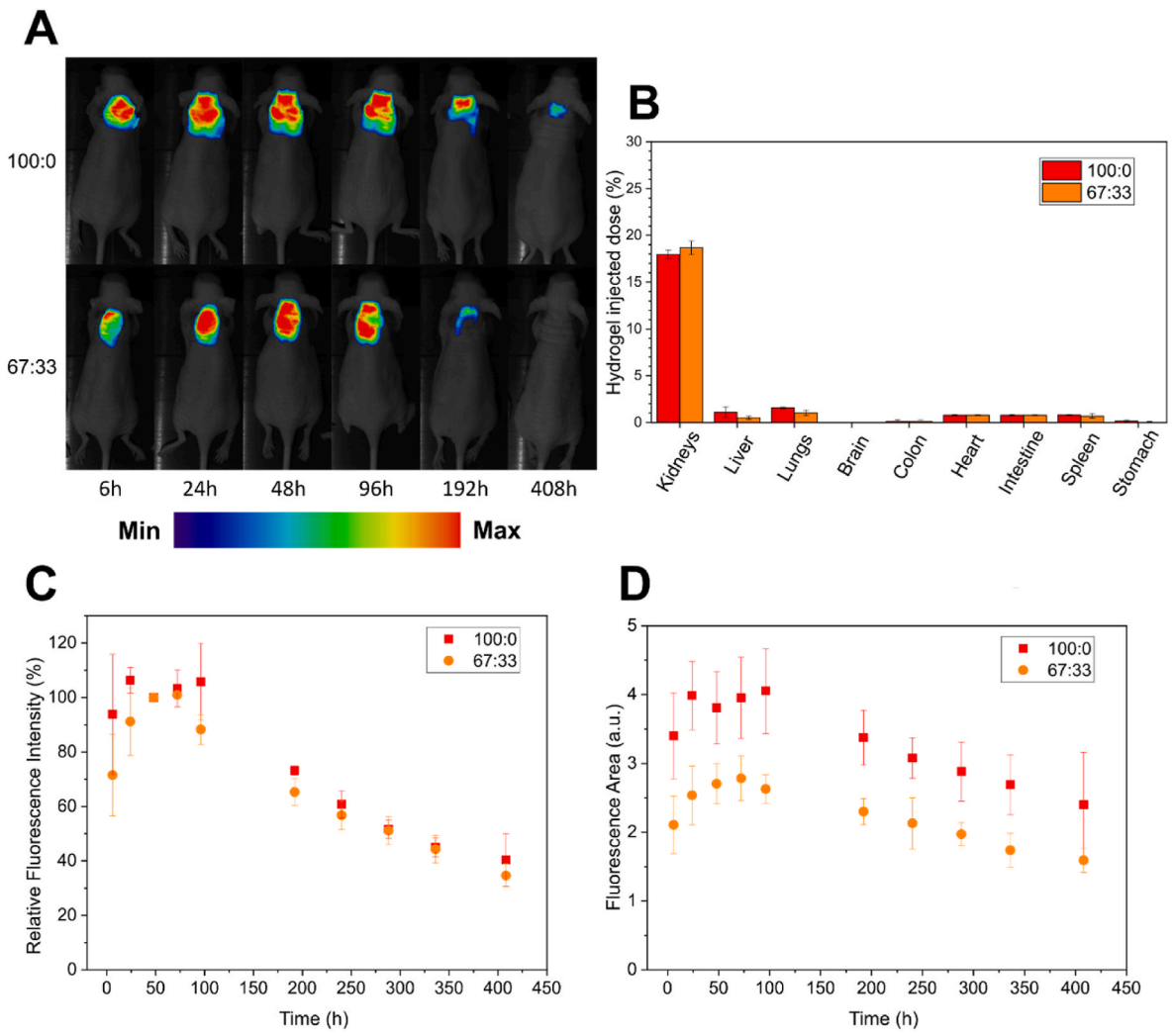

Fig. 5. Assessment of the *in vivo* biodegradability and bio elimination of two different formulations of hydrogels at 5 % w/w. **A)** Fluorescent degradation patterns associated to the 67:33 % and 100:0 % chitosan@DOTAGA:chitosan formulations until day 17 evidencing the effective biodegradability of the gel after SC injection of 150 μL in nude mice (n = 3, the images are examples), **B)** Residual hydrogel fraction assessed by ICP-MS Biodistributions of Gd^{3+} in mice organs after injection of formulations complexed with gadolinium (70 % of the DOTAGA). This study revealed no undesired accumulation in organs other than the expected renal clearance pathway (mean ± SD), **C)** and **D)** Relative fluorescence intensity and fluorescence area related to the fluorescent signals recorded for these formulations from injection to day 17. A similar degradation pattern is observed with a tighter area for the more viscous 67:33 % formulation (mean ± SD).

characterized this foreign body reaction by a central area populated by mononuclear cells (predominantly macrophages), surrounded by lymphocytes and eosinophils, along with the presence of mature connective tissue. In animals observed for 10 and 11 weeks (Groups 3 and 4), an increase in lymphocyte cellularity was noted in axillary and/or cervical lymph nodes, likely representing a secondary delayed response to the chronic inflammation. These findings suggest that the 67:33 % injectable hydrogel formulation undergoes a slow degradation process, primarily mediated by macrophages, a common systemic response to injected foreign materials [44,45]. Importantly, the absence of systemic toxicity or local irritation at the injection site underscores the biocompatibility and tolerability of the formulation, even as it persists as a depot at the site of administration up to 11 weeks post-injection.

3. Conclusions

In this study, we highlighted the potential of chitosan@DOTAGA:chitosan injectable hydrogels as a versatile platform for various biomedical applications. Our findings reveal that the functionalization of chitosan with DOTAGA plays a key role on the modification of charges along the polymer backbone, which enables the formation of physical crosslinks in response to an increase of pH and osmolarity, leading to the *in situ* formation of an hydrogel in physiological conditions. We evidenced the crucial interest of mixing chitosan@DOTAGA with unmodified chitosan to form a stable hydrogel that is strengthened by crystallization and hydrophobic interactions provided by chitosan. Rheological studies, microstructural analyses and morphology observations shed light on the possibility to tune the hydrogel's physicochemical properties by modifying the relative amount of the two polymers in the formulation. *In vivo* experiments on mice models confirmed this finding using MRI and fluorescence imaging. Finally, the preclinical tolerability of these formulations was validated after SC administration on rabbits in a GLP environment. Building on the use of these hydrogels for immunotherapy delivery, this work paves the way for broader applications, including the controlled release of a wide range of drugs, as well as the development of dermal fillers.

4. Experimental section

Materials: Medical grade chitosan used in this study has been purchased from Matexcel (Bohemia, NY, USA, reference number NAT-0030) and is of animal origin (Alaska snow crab). It was characterized

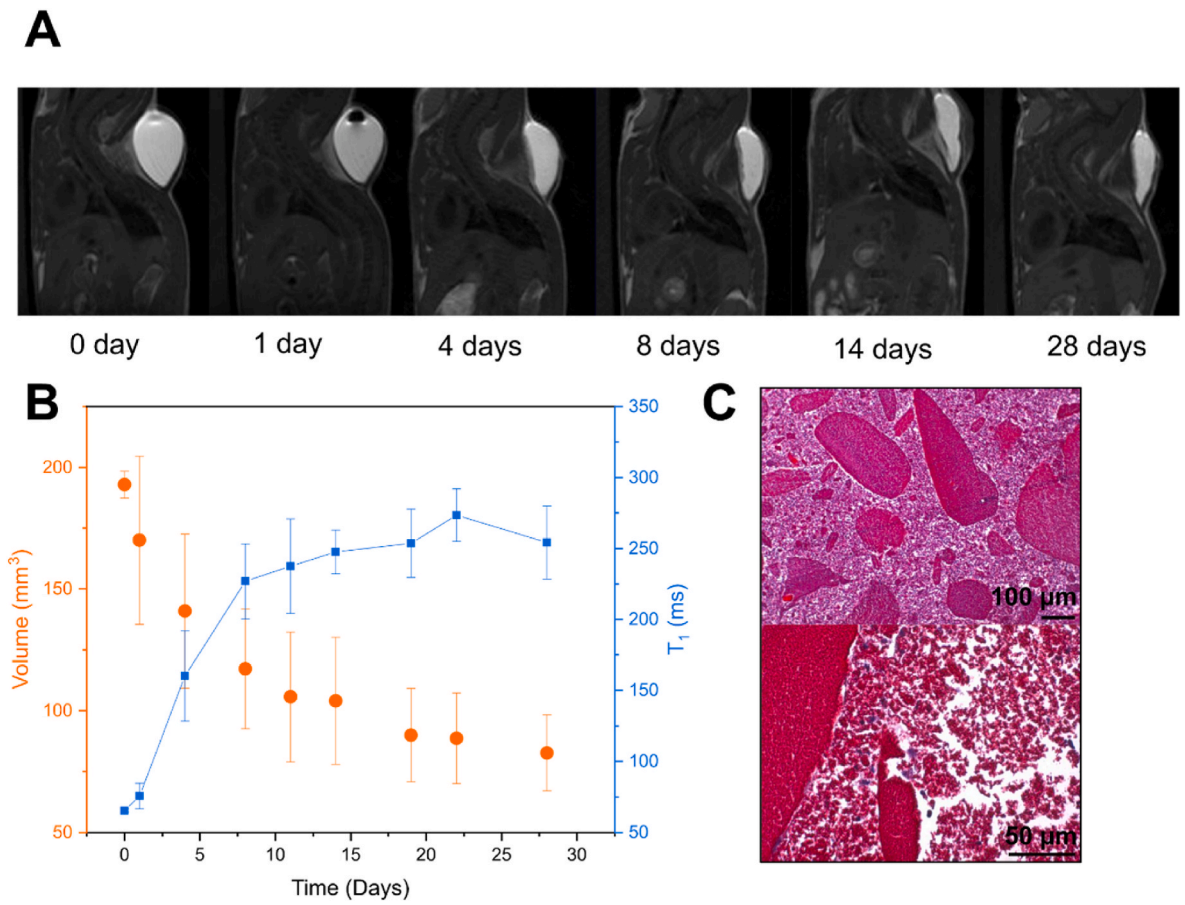

Fig. 6. Evaluation of the biodegradation of chitosan@DOTAGA:chitosan 67:33 % at a concentration of 5 % w/w after subcutaneous injection (SC) in mice (the formulation contains chitosan@DOTAGA precomplexed with Gd^{3+} in the concentration 300 ppm of Gd in the final solution) **A)** T_1 weighted MRI images of sagittal section of mice within the study, **B)** Evolution of scaffold volume (in mm^3) and T_1 values (in ms) during the 28-day study, **C)** Hematoxylin & eosin (H&E) staining of the SC tissue at day 28 after injection of the hydrogel (two different magnifications).

by ^{1}HNMR [26] to obtain the mean degree of acetylation and the molar masses were determined by SEC-MALLS. DOTAGA anhydride was provided by CheMatech (Dijon, France). Acetic acid was supplied from VWR (France). 1,2-propanediol, acetic anhydride and all other chemicals were purchased from Sigma-Aldrich (France), were of analytical grade and used as received.

Synthesis of Chitosan@DOTAGA: The synthesis was performed as described by Gréa et al. [25]. 60 g of chitosan were introduced into a 10 L reactor with 4 L of MilliQ water and 50 mL of glacial acetic acid, then the mixture was placed under mechanical stirring at 500 rpm. After the complete dissolution of the chitosan (3 h), 4 L of 1,2-propanediol were added to the medium and the mixture was kept under stirring until homogenization (2 h). 120 g of DOTAGA anhydride were then added ($n_{DOTAGA}/n_{NH2} = 0.75$), and the mixture was kept under stirring overnight. The synthesis product was then purified by tangential filtration using the Sartoflow® Advanced device with a Sartocon® Slice PESU cassette (polyethersulfone membranes; cut-off: 100 kDa; filtration area: 0.1 m^2) against 200 L of a 0.1 mol/L acetic acid solution, and then against 200 L of a 5 mmol/L acetic acid solution (pH = 4.6). The resulting product was freeze-dried in a LYOVAC brand freeze-dryer for 162 h including 50 h of secondary drying and recovered in the form of a spongy solid. After lyophilization, the measurement of residual moisture content and water activity was carried out on the solution. Water content was determined by heating the sample followed by Karl Fischer titration. (Anolyte Hydranal –Coulomat AG oven (Riedel de Haën), speed 45 %, mixing 60 s, set temperature 140 °C). The values of the different water activities of the samples were measured using an AQUALAB device which uses the chilled mirror dew point technique. The chitosan@DOTAGA samples exhibit high a residual humidity close to 7.5 % ± 0.3 % with a water activity of 0.19 at 20 °C.

HPLC-SEC-MALLS Molar masses, Polydispersity and Gyration Radius Determinations: Molar mass distributions were determined with a SEC-MALLS configuration at the Chromatography Plateform of Chemistry Institute of Lyon (ICL) comprising a VWR degasser, an Agilent 1260 Infinity pump whose flow rate is fixed at 0.5 mL/min, an Agilent 1260 Infinity ALS automatic injector (typical injected volume: 100 µL), an Agilent 1260 Infinity TCC oven (Temperature = 30 °C), a detector UV Agilent1260 Infinity MWD VL (λ = 280 nm), a Wyatt DAWN HELEOS II MALLS detector (laser λ = 664 nm, Fused Silica cell), a Wyatt Optilab T-rex refractometer with λ = 658 nm (thermostated at 25 °C), 2 columns: TSK PW G6000 and TSK PW G2500 (Tosoh). The analysis was carried out with a 0.2 mol/L acetate buffer eluent (pH = 4.8), an analysis time of 60 min and samples at a concentration of 1 mg/mL. To perform the SEC analysis, the samples were first filtered through a 0.45 µm CME filter. The dn/dc = 0.193 mL/g ratio was determined on samples in the concentration range from 0.1 mg/mL to 1 mg/mL prepared using the buffer solution and previously filtered on a 0.1 µm Cellulose Acetate/Cellulose Nitrate filter.

HPLC-SEC-UV Purification follow-up: HPLC-SEC chromatograms were recorded with a Shimadzu Prominence HPLC system at an operating temperature of 30 °C. The SEC column used was a PolySep-GFC-P 4000 column and the eluent used was 0.1 mol/L solution of acetic acid/0.1 mol/L ammonium acetate buffer. The absorption wavelength of the UV detector was set to 295 nm and the eluent flow rate was set to 0.8 mL/min. A retention time of 7.7 min is measured for chitosan@DOTAGA and a peak at 11.3 min is observed for ungrafted DOTAGA. The purification

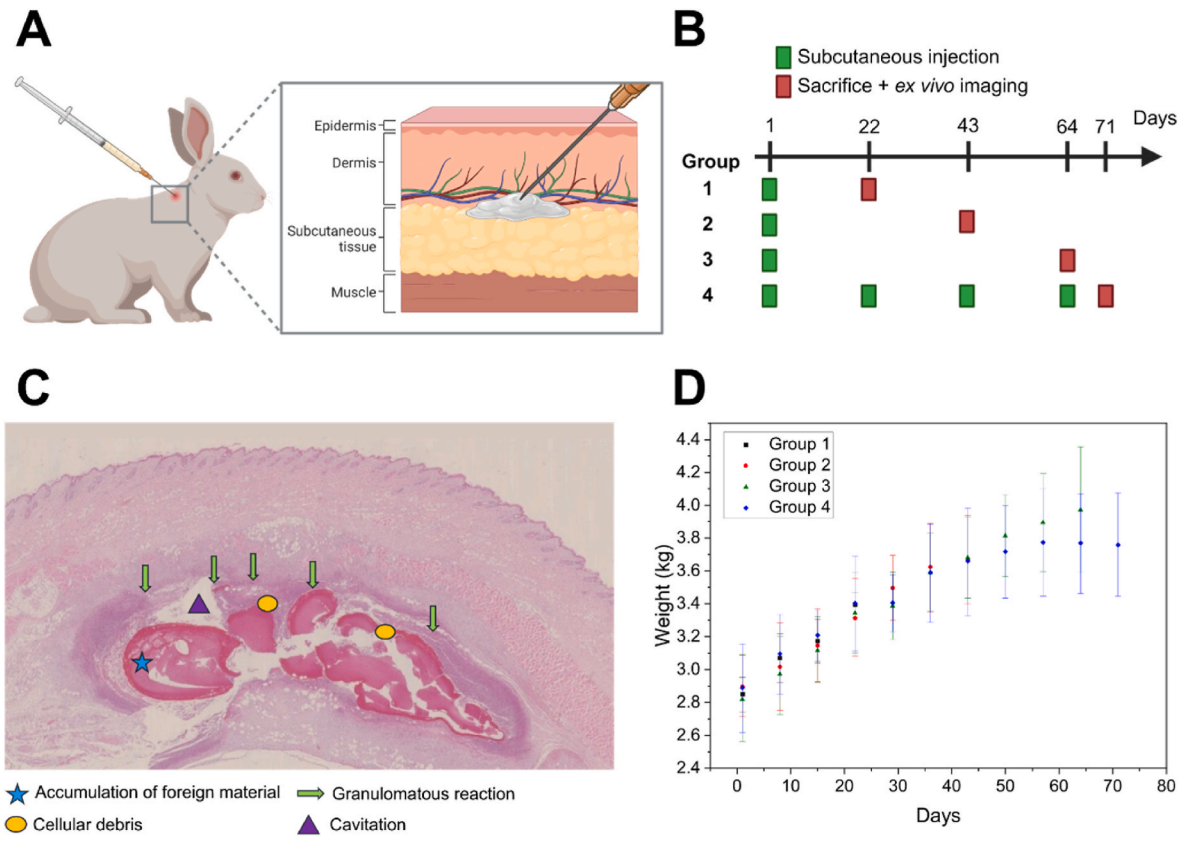

Fig. 7. Assertion of the local safety and tolerance study (GLP compliant) of the 67:33 % formulation in rabbits. **A)** Scheme of the chosen SC injection route chosen for the tolerance study with subcutaneous injections in the scapular region of rabbits, **B)** Timeline of hydrogel administration and sacrifice for the 4 groups with single or multiple subcutaneous injections, **C)** Optical microscopy images of sections (dermis and subcutis) after Hematoxylin and Eosin staining with indications of the foreign body reaction, **D)** Evolution of bodyweight during the study for the four groups highlighting no macroscopic toxicity of the formulation after subcutaneous injection in rabbits.

in % is determined by using the ratio of the area of the peak corresponding to the free DOTAGA to the total area of the two peaks.

Determination of Degree of Substitution by Copper (Cu^{2+}) Dosage: Copper chelation studies [28] have been conducted on the freeze-dried product re-dissolved in a 0.1 mol/L acetate buffer (pH = 4.53) to evaluate the copper extraction capacity as well as to estimate the degree of substitution (*DS*) of DOTAGA in the synthesized product. A suitable volume of buffer solution was introduced into a vial to obtain a sample whose total volume is 2 mL. 200 μL of chitosan@DOTAGA at 10 g/L were then introduced into each vial containing the buffer solution beforehand and a different amount of a 15 mmol/L aqueous solution of $CuCl_2$ was added. The vials containing the samples were then homogenized by stirring using a vortex. In practice, copper concentrations ranging from 0 to 1 mmol/L have been investigated. The absorbance of all samples at $\lambda = 295$ nm has been recorded using a UV–Vis spectrophotometer by plotting the evolution of absorbance with copper concentration. The crossover between the partial chelation and saturation regimes yields the maximum copper chelation capacity at $C^*_{Cu2+} = 0.65$ mmol/L, which corresponds to a copper absorption capacity of 42 mg/g of chitosan@DOTAGA. By making the correction relating to the residual humidity rate of 7.5 % measured previously on the chitosan@DOTAGA lyophilizate, we obtain a copper uptake capacity of 45 ± 1 mg/g which corresponds to an estimated *DS* of 17.1 ± 0.5 %.

Solubility Studies: The determination of the solubility range was carried out on solutions with total polymer concentration of ~1 w/w %. A 1 % w/w stock solution of 100 mL was produced by dissolving the polymer(s) in an aqueous solution of acetic acid where the pH has been adjusted to pH = 5.4 by adapting the quantity of glacial acetic acid. 10 mL of the stock solution were introduced into different vials and then pH was varied from pH = 4 to pH = 9 by controlled addition of NaOH and HCl solutions at 1 mol/L 1 mL of each solution was then dispatched into several vials and a 2 mol/L NaCl solution was added to each vial in order to vary the osmolarity to 50, 150, 250 and 350 mOsm/L. The osmolarity of the solution at pH = 4, before addition of the salt solution, was determined using a Löser Micro Osmometer MOD200 Plus from Camlab and was estimated to be 12 mOsm/L. Prior to measurement, zero was set using 15 μL of distilled water, and the instrument was calibrated against 15 μL of a 300 mOsm/kg standard. The sample was measured by taking a volume of 15 μL frozen to −6.0 °C. The solubility was determined qualitatively by turbidity observation. Images of the vials prepared for the solubility studies are displayed in the supplementary data section (Fig. S10).

Formulation of chitosan@DOTAGA:chitosan Mixtures: These mixtures were prepared at 5 % w/w total polymer concentration by addition of chitosan@DOTAGA, chitosan, MilliQ water and glacial acetic acid. Chitosan@DOTAGA and chitosan amounts were adapted to reach the different ratios between the two polymers concentrations (*i.e.* chitosan@DOTAGA:chitosan 100:0 %, 83:17 %; 67:33 %, 50:50 %, 0:100 % ratios). In the same way, the quantity of acetic acid was adapted for each formulation in order to solubilize the polymers as follows: the concentration of acetic acid was 1.6 % w/w for 0:100 % formulations, 0.6 % w/w for 50:50 % formulations, 0.4 % w/w for 67:33 % formulations, 0.2 % w/w for 83:17 % formulations, and no acetic acid was added for 100:0 % formulations. The mixtures were placed in a 50 mL reactor and kept under mechanical stirring at 100 rpm for 2 h. The obtained solutions were centrifuged at 3400*g for 10 min to obtain air bubble-free solutions and introduced into glass syringes with a Nordson Optimus fluid dispenser, then sterilized for 20 min at 121 °C in an autoclave.

Rheological characterization and Flow behavior: Rheology studies were conducted on a Thermo Scientific HAAKE RheoStress 600 Sensor Systems using a C35/2° cone plate geometry. The gap was set to 105 μm. The sample's surplus was removed using a spatula to limit the edge effects. The viscosity of each sample was measured with a flow sweep study varying the shear rate from 10^{-2} to 10^{3} s^{-1} at a regulated temperature of 25 °C. 10 points per decade were recorded. The Newtonian viscosity is defined as the average value of the viscosity measured at the plateau evidenced at low shear rates.

Determination of the Injectability of solution formulations: Injectability of samples were determined using a Shimadzu AG-X plus force machine equipped with a 10 kN cell to measure the force required to compress at a set rate the plunger of a syringe containing the solutions. Syringes equipped with needles and containing the solution were thus introduced into a support with a chamber of the size of the outer diameter of the syringe. The syringe was fixed with three axial polyamide screws to keep the system stable and aligned with the piston during compression. A scheme of the system is proposed in the supplementary data section (Fig. S11). The syringes used were BD Hylok™ glass pre-fillable syringe of 1 mL. Injectability measurement was conducted at a speed rate of 60 mm/min by measuring the necessary force to maintain the piston speed rate. Reported ejection forces are the average force value measured over 5 s after a stable force is obtained. Needles used for this study were Terumo® Agani™ Needles 25G (0.50 × 16 mm) with a measured internal diameter of 284.3 μm determined by electron microscopy (Fig. S12). Extended viscosity diagram was established by applying plunger speed ranging from 100 mm/min to 0.01 mm/min and waiting for a constant force to be measured for each step. The setup worked to determine the capillary viscosity. Detailed equations used for calculation are provided elsewhere [15].

Gel Formation Kinetics and Viscoelastic Properties: Approximately 2 mL of the formulation were placed into a round mold with an inner diameter of 25 mm and a height of 3 mm. The mold containing the solution was then immersed in 50 mL of PBS at 10 mmol/L to start the gelation process of the solution. The storage (G') and loss (G'') shear moduli of the formed hydrogel were recorded on an ARES rheometer (TA instruments) using a 25 mm plate geometry. Prior to measurements, the zero fixture was achieved by placing an empty mold with double-sided tape on the lower part of the geometry. A preliminary study was carried out on hydrogels with a dynamic strain sweep test by varying the strain amplitude from 0.1 % to 100 % at a fixed frequency of 10 rad/s at 25 °C. Fixing the strain amplitude to 1 % ensured that the measurements are carried out in the linear viscoelastic regime (Fig. S13). Oscillatory rheological properties were then measured aligning the axis of upper plate and the placed mold containing the hydrogel with a dynamic frequency sweep test from 0.05 rad/s to 100 rad/s at 25 °C. Measurement at different time points were achieved on different gels to ensure that the measurement would not affect rheological properties of the material.

4.1. Microstructure study by synchrotron SAXS and WAXS

Small Angle X-ray Scattering and Wide Angle X-ray Scattering measurements were performed at the ESRF (European Synchrotron Radiation Facility, Grenoble, France) on the D2AM BM02 beamline. Polymer solutions were prepared by addition of chitosan@DOTAGA and chitosan in different mass ratios (100:0 %, 67:33 % and 0:100 %). The total polymer concentration was fixed to 5 % w/w. Hydrogels were prepared by filling of stainless-steel washer cells (internal diameter: 4 mm, width: 3 mm) covered with adhesive Kapton® foil on one side, with the different polymer solutions. The cells were then immerged in the coagulation bath (either 10 mM phosphate buffer, 10 mM phosphate buffered saline or 0.9 % sodium chloride solutions) for 24 h, then sealed with another piece of Kapton foil and finally stored wrapped in parafilm to avoid air drying of the samples.

For WAXS analysis, the apparent crystallite sizes were estimated using the Scherrer equation (Murthy, 2016):

$$D_{200} = \frac{2\pi}{\Delta q_{200}}$$

where D_{200} is the size of the crystallites in the direction perpendicular to the reflecting *(200)* family of planes and Δq_{200} is the full width at half maximum of the WAXS crystallinity peak located close to $q_{200} = 1.4$ $Å^{-1}$.

Hydrogel Sample Preparation and SEM Imaging: 500 μL of the solution formulations were injected into 100 mL of PBS at 10 mmol/L with a 25 G needle. After gelling for 1 h, the medium was replaced with a 20 % v/v solution of ethanol in water. Every hour, the solution was replaced by a solution in which the ethanol concentration gradually increases by 20 % v/v until the gel was immersed in pure anhydrous ethanol 4 h after the first exchange of solutions. The Critical Point Drying (CPD) method as well as the imaging was carried out at the "Centre Technologique des Microstructures (CTμ)". The gel was dried using the CPD method by carrying out 12 cycles of 120 s at 18 °C to pass from ethanol to gaseous CO_2. Once dried, the sample was placed on a metallic stub. A coating of 10 nm of copper on the surface of the samples was carried out with a MED 020 BAL-TEC high vacuum setup. The observation was then achieved on a SEM FEI QUANTA 250 FEG at 2 kV. For the slice observation, a LN2 fracture was achieved on the sample after CPD by immersing the gel in liquid nitrogen.

Refraction Index CellExplorer microscopy Sample Preparation, Imaging and Processing: About 500 μL of the solution formulations were dropped onto a microscope slide (Corning®), then spread using a metallic spatula. The slide was then immerged in a 10 mM phosphate-buffered saline solution until complete gelation of the polymer. The gel was then covered by a coverslip before imaging. Imaging was performed on a 3D Cell Explorer Fluo (Nanolive SA). Images were processed using *ImageJ* software to extract line profiles further used to calculate autocorrelation functions (using *xcorr()* under Octave programming environment). More precisely, *Oxz* sagittal images were obtained by reconstruction using the 96 *Oxy* frontal slices spaced 0.3 μm apart. Gray-level signals of these *Oxz* sagittal and *Oxy* frontal images were obtained by plotting gray-level values as a function of position (in μm) on the image. After calculation of autocorrelation functions (acf), the smallest length L_1 was determined as the intercept of the initial tangent of the ACF and the horizontal plateau at the minimum of acf. The periodicity distance or long period L_p was determined as the first local maximum exhibited after the initial decrease of acf, as shown on Fig. S7. A second characteristic distance L_2 can be extracted from $L_p = L_1 + L_2$. Size attribution (i.e. size of pores or sizes of surrounding material) was deduced from observation of the images. There were 477 Gy-levels plots per formulation with a distance of 0.2 μm between two successive gray-level analyses. L_1 and L_p values presented are the averages of the 477 characteristic lengths obtained by the autocorrelation calculation. Resulting pore and matter sizes are reported in Table S1.

Chitosan@DOTAGA Labellings: chitosan@DOTAGA was labelled with Cyanine 5.5 by direct addition under stirring of a 5 g/L cyanine 5.5 NHS ester (Sigma Aldrich) solution on a 1 % w/v chitosan@DOTAGA solution whose pH was adjusted to 6 ($n_{CyanineNHS}/n_{NH2} = 0.037$) using a 0.1 mol/L sodium hydroxide solution. The reaction mixture was left for 24 h under stirring in the dark. The synthesis product was then purified by tangential filtration using the Sartoflow® Smart device with a Sartocon® Slice PESU cassette (polyethersulfone membranes; cut-off: 100 kDa; filtration area: 200 cm^2) against 10 L of a 5 mmol/L acetic acid solution. The synthesis product was then freeze-dried for 48 h with a Büchi L-200 pro freeze dryer. Complexation of chitosan@DOTAGA with Gd^{3+} cations was achieved by direct addition of a 1 mol/L solution of $GdCl_3$ into a chitosan@DOTAGA solution: 8.74 mL of a 1 mol/L solution of Gd^{3+} were added to 1 L of a 7 g/L solution of chitosan@DOTAGA under stirring ($n_{Gd}/n_{DOTAGA} = 1.2$). The pH was then adjusted from pH = 3.6 to pH = 5.6 by addition of a 1 mol/L sodium hydroxide solution. The solution was left under agitation at 60 °C for 48 h. Again, the

synthesis product was then purified by tangential filtration using the Sartoflow® Smart device with a Sartocon® Slice PESU cassette (polyethersulfone membranes; cut-off: 100 kDa; filtration area: 200 cm^2) against 10 L of a 5 mmol/L acetic acid solution. The purified product was then lyophilized for 48 h with a Büchi L-200 pro freeze dryer. The amount of gadolinium complexed onto the grafted chelating group of chitosan@DOTAGA was measured by ICP-MS ^{158}Gd analysis conducted on a PerkinElmer NexION 2000. It was estimated that 70 % of the total DOTAGA groups were complexed with gadolinium.

In Vivo Degradability of hydrogels with Fluorescent Follow-up and Gd^{3+} Biodistribution Determination: Animal experiments were approved by the CLB-CRCL CE010 (Lyon) Animal research committee (Approval No. APAFIS #43973–2023051711386841 v6). Healthy NMRI Nude mice (~9 weeks old) were used for the experiment. For this study, chitosan@DOTAGA was grafted with a Cyanine 5.5 fluorescent dye to perform fluorescence imaging and labelled with gadolinium ions Gd^{3+} for ICP measurements (as described in the previous section). 150 μL of the studied formulation were injected subcutaneously in nude mice ($n = 3$). Fluorescence images as well as bright-field images were acquired via a back-thinned CCD-cooled camera ORCAIIBT-512G (Hamamatsu Photonics Deutschland GmbH, Herrsching am Ammersee, Germany) using a colored glass long-pass RG 665 filter (Melles Griot, Voisins les Bretonneaux, France). Optical excitation was carried out at 633 nm, and the emission was detected at a wavelength of 680 nm. Exposure time was set at 30 s for optical imaging and 0.05 s for bright field imaging. Fluorescence images were acquired at different timepoints to monitor the loss of fluorescence over time resulting in the degradation of the hydrogel. Images were analyzed using FIJI ImageJ software with Java version 1.8.0_172. The quantification of fluorescence signal in each organ was performed following an ImageJ macro that selects automatically the ROI using a threshold and extracts ROI values (ROI area, total fluorescence intensity, fluorescence density). 17 days after administration, mice were anesthetized and sacrificed through cervical dislocation. Tissues close to the administration site (skin, muscle, remaining gel if any) as well as other organs (stomach, intestines, colon, blood, urine, kidneys, liver, brain, spleen, heart, lungs) were harvested for *ex vivo* Gd^{3+} quantification. A Multiwave 5000 Anton Paar microwave was used for tissues and organs digestion. Organs were divided and digested according to their weights to ensure homogeneity of digestion throughout the method. Standard 69 % HNO_3 and ultrapure water were used for all digestion and sample preparation. Reactors were cleaned before and after sample cycles with the programmed cleaning method (4 mL water and 6 mL 69 % HNO_3, 0–180 °C ramping over 10 min, 180 °C for 10 min) and rinsed with ultrapure water after each cycle. Samples were then digested using the Bio-Organic Digestion Method (69 % HNO_3, 0–100 °C ramping over 10 min, 100 °C for 10 min, 100–200 °C ramping over 10 min, and 200 °C for 10 min). ICP-MS analyses were carried out on a PerkinElmer NexION. Before use, the machine was cleaned continuously with 10 % HNO_3 for 20 min then with 1 % HNO_3 for 1.5 h. All the system parameters were optimized before beginning the analysis following the machine's protocols (mass calibration, torch alignment, QID in mode KED and standard, nebulizer gas flow, and dual detector calibration). Once all of the parameters are optimized, a final performance check was done in standard and KED. An internal standard of 2 ppb Indium was used in all ICP samples to ensure a consistent measurement and reliability. The base solvent was composed of 0.5 % HNO_3, 0.7 % tert-butanol, and ultrapure water. The tert-butanol was included to help minimize the matrix effects of carbon, since degradation of the samples included proteins and other carbon-heavy biomolecules. Gadolinium (^{158}Gd) amount was then analyzed in each sample.

In vivo Degradability of hydrogels by MRI using Gd^{3+}-complexed chitosan@DOTAGA: This preclinical study was reviewed and approved by the Turin Animal Testing Ethics Committee (protocol CC652.167. EXT.52 dated December 06, 2021, within the research project authorized with n°888/2021-PR dated November 15, 2021). Injections, MRI imaging, T_1 and T_2 analysis and histological analysis were carried out at the Molecular Imaging Center of the Department of Molecular Biotechnology and Health Sciences at the University of Turin. Approximately 200 μL of the formulation was injected subcutaneously into the backs of healthy BALB/c mice using 22 G needles. Magnetic resonance images of the implanted hydrogel were recorded up to 1 month after implantation at 7.1 T on a Bruker Avance Neo 300 MHz spectrometer equipped with a micro 2.5 imaging probe at room temperature. Signal intensity in the liver, kidneys and spleen was also monitored. T_{2W} (T_2-weighted) images were acquired using a standard RARE (Rapid Acquisition with Refocused Echoes) sequence with the following parameters: repetition time - $TR = 4000$ ms (interval between two excitations), echo time - $TE = 24$ ms (time interval between excitation and occurrence of MRI signal), RARE factor = 16, number of averages = 4, Field Of View $FOV = 30$ mm, slice thickness = 1 mm, matrix size 128 × 128. T_{1W} (T_1-weighted) images were acquired using a standard MSME (multi spins multi echoes) sequence with the following parameters: $TR = 400$ ms, TE = 3.3 ms, number of averages = 6, $FOV = 30$ mm, slice thickness = 1 mm, matrix size 128 × 128. T_1 values were measured using a spin echo sequence with saturation recovery ($TE = 3.8$ ms, 10 variable TRs ranging from 50 to 5000 ms, $FOV = 30$ mm, slice thickness = 1 mm, matrix size 128 × 128) and analyzed using the T_1 saturation recovery equation. Hydrogel size was measured by manually trimming the region of interest on the magnetic resonance images. Dissection was held 30 days post-injection, and hydrogel fragments were collected, stained with hematoxylin and eosin according to a standard protocol, and imaged by light microscopy.

In Vivo Subcutaneous Local Tolerance: This study was conducted in compliance with the Good Laboratory Practice (GLP) regulations (US FDA [21 CFR part 58, December 22, 1978] and subsequent revisions; Directive 2004/10/EC of the European Parliament and of the Council of February 11, 2004; ENV/MC/CHEM(98)17 "OECD principles on Good Laboratory Practice – as revised in 1997"; Decreto Legislativo no. 50 of March 2, 2007 and subsequent revisions, study n°A4670, protocol approved on September 29, 2022). The study design was based on ISO 10993–6:2016(E) standard and CPMP/SWP/2145/00 Rev.1 guideline on non-clinical local tolerance testing of medicinal products. 500 μL of the studied formulation was administered as a single or repeated subcutaneous injections in the scapular region of New Zealand White Specific Pathogen Free (SPF) nulliparous and non-pregnant female rabbits [*Crl:KBL(NZW)*]. After the scheduled test period, animals were sedated with Dorbene Vet® and perfused by intravenous injection of Tanax®. Histopathological examination was performed on each preserved injection site and draining lymph nodes (cervical and axillary nodes). Sections were processed by dehydration and embedding in paraffin wax. Sections of 5 μm thickness were cut, stained with hematoxylin and eosin and mounted onto glass slides for examination.

CRediT authorship contribution statement

Arthur Durand: Writing – original draft, Validation, Investigation, Conceptualization. **Thomas Gréa:** Writing – original draft, Investigation, Conceptualization. **Gabin Lebeau:** Investigation. **Guillaume Jacquot:** Investigation, Data curation. **Augustin Tillement:** Investigation, Data curation. **Axel Aigle:** Methodology, Formal analysis, Conceptualization. **Eloïse Thomas:** Methodology, Investigation, Data curation, Conceptualization. **David Kryza:** Validation, Supervision. **Jacqueline Taleb:** Supervision, Methodology. **Giuseppe Ferrauto:** Supervision, Methodology, Investigation. **Eliana Gianolio:** Validation, Methodology, Investigation, Conceptualization. **Alain Géloën:** Methodology, Investigation, Conceptualization. **Alexandra Montembault:** Validation, Methodology, Conceptualization. **Maria Gutiérrez-Blanco:** Validation, Methodology. **Xavier Pivot:** Validation, Resources, Methodology, Conceptualization. **Sébastien Harlepp:** Writing – review & editing, Supervision, Methodology, Conceptualization. **Alexandre Detappe:** Writing – review & editing, Validation, Supervision, Resources, Methodology, Conceptualization. **Laurent David:** Writing – review & editing, Validation, Supervision, Resources, Project administration,

Conceptualization. **François Lux:** Writing – review & editing, Validation, Supervision, Resources, Project administration, Methodology, Conceptualization. **Olivier Tillement:** Writing – review & editing, Validation, Supervision, Resources, Project administration, Methodology, Conceptualization.

Declaration of competing interest

T.G., A.A., A.M., L.D., F.L., O.T., are inventors on a patent concerning the hydrogel formulation described in this work (FR3127759A1). A. Du. and A.A. are employees of MexBrain company. F.L. and O.T. possess shares in the Mexbrain company. G.J. and A.T. are employees of Nano-H company. The other authors declare no conflict of interest.

Acknowledgements

A.Du. and T.G. contributed equally to this Work. This study was performed in the frame of the project HYDROPEP with the financial support of the Région Auvergne Rhône- Alpes (Project Number 22 01859401). The authors are grateful to the "Centre Technologique des Microstructures (CTμ)" (Villeurbanne, FRANCE). We thank AbbVie Allergan company (Annecy, France) for the gift of the Haake RheoStress 600 rheometer. The authors acknowledge Euro-Bioimaging (www.eurobioimaging.eu) for providing access to imaging technologies and services via the Molecular Imaging Italian Node (Torino, Italy). A. De. acknowledges support from the Ligue contre le cancer, as well as the European Research Council (ERC) under the European Union's Horizon 2020 research and innovation program. This includes the ERC Starting Grant TheranoImmuno (grant agreement No. 950101) and the ERC Proof-of-Concept Grant Sub-NK (grant agreement No. 101138078). Fig. 7A was obtained using Biorender.com.

Appendix B. Supplementary data

Supplementary data to this article can be found online at https://doi.org/10.1016/j.mtadv.2025.100565.

Data availability

Data will be made available on request.

References

[1] A. Mellati, J. Akhtari, Injectable hydrogels: a review of injectability mechanisms and biomedical applications, RMM 6 (2019) 1–14, https://doi.org/10.18502/rmm.v6i4.4799.
[2] L. Liu, Q. Gao, X. Lu, H. Zhou, In situ forming hydrogels based on chitosan for drug delivery and tissue regeneration, Asian J. Pharm. Sci. 11 (2016) 673–683, https://doi.org/10.1016/j.ajps.2016.07.001.
[3] S. Ishikawa, K. Iijima, D. Matsukuma, M. Iijima, S. Osawa, H. Otsuka, An interpenetrating polymer network hydrogel with biodegradability through controlling self-assembling peptide behavior with hydrolyzable cross-linking networks, Materials Today Advances 9 (2021) 100131, https://doi.org/10.1016/j.mtadv.2021.100131.
[4] Y. Sun, D. Nan, H. Jin, X. Qu, Recent advances of injectable hydrogels for drug delivery and tissue engineering applications, Polym. Test. 81 (2020) 106283, https://doi.org/10.1016/j.polymertesting.2019.106283.
[5] W. Hu, Z. Wang, Y. Xiao, S. Zhang, J. Wang, Advances in crosslinking strategies of biomedical hydrogels, Biomater. Sci. 7 (2019) 843–855, https://doi.org/10.1039/C8BM01246F.
[6] A. Mandal, J.R. Clegg, A.C. Anselmo, S. Mitragotri, Hydrogels in the clinic, Bioengineering & Translational Medicine 5 (2020) e10158, https://doi.org/10.1002/btm2.10158.
[7] C.I. Nkanga, A. Fisch, M. Rad-Malekshahi, M.D. Romic, B. Kittel, T. Ullrich, J. Wang, R.W.M. Krause, S. Adler, T. Lammers, W.E. Hennink, F. Ramazani, Clinically established biodegradable long acting injectables: an industry perspective, Adv. Drug Deliv. Rev. 167 (2020) 19–46, https://doi.org/10.1016/j.addr.2020.11.008.
[8] X. Wang, D.J. Burgess, Drug release from in situ forming implants and advances in release testing, Adv. Drug Deliv. Rev. 178 (2021) 113912, https://doi.org/10.1016/j.addr.2021.113912.
[9] S. Almawash, S.K. Osman, G. Mustafa, M.A. El Hamd, Current and future prospective of injectable hydrogels—design challenges and limitations, Pharmaceuticals 15 (2022) 371, https://doi.org/10.3390/ph15030371.
[10] Z. Ahmad, S. Salman, S.A. Khan, A. Amin, Z.U. Rahman, Y.O. Al-Ghamdi, K. Akhtar, E.M. Bakhsh, S.B. Khan, Versatility of hydrogels: from synthetic strategies, classification, and properties to biomedical applications, Gels 8 (2022) 167, https://doi.org/10.3390/gels8030167.
[11] Y. Li, H.Y. Yang, D.S. Lee, Biodegradable and injectable hydrogels in biomedical applications, Biomacromolecules 23 (2022) 609–618, https://doi.org/10.1021/acs.biomac.1c01552.
[12] S. Peers, A. Montembault, C. Ladavière, Chitosan hydrogels for sustained drug delivery, J. Contr. Release 326 (2020) 150–163, https://doi.org/10.1016/j.jconrel.2020.06.012.
[13] G. Tang, Z. Tan, W. Zeng, X. Wang, C. Shi, Y. Liu, H. He, R. Chen, X. Ye, Recent advances of chitosan-based injectable hydrogels for bone and dental tissue regeneration, Front. Bioeng. Biotechnol. 8 (2020) 587658, https://doi.org/10.3389/fbioe.2020.587658.
[14] S. Alven, B.A. Aderibigbe, Chitosan and Cellulose-Based Hydrogels for Wound Management, vol. 21, IJMS, 2020, p. 9656, https://doi.org/10.3390/ijms21249656.
[15] C. Halimi, A. Montembault, A. Guerry, T. Delair, E. Viguier, R. Fulchiron, L. David, Chitosan solutions as injectable systems for dermal filler applications: rheological characterization and biological evidence, in: 2015 37th Annual International Conference of the IEEE Engineering in Medicine and Biology Society (EMBC), IEEE, Milan, 2015, pp. 2596–2599, https://doi.org/10.1109/EMBC.2015.7318923.
[16] S. Ladet, L. David, A. Domard, Multi-membrane hydrogels, Nature 452 (2008) 76–79, https://doi.org/10.1038/nature06619.
[17] A. Montembault, C. Viton, A. Domard, Rheometric study of the gelation of chitosan in aqueous solution without cross-linking agent, Biomacromolecules 6 (2005) 653–662, https://doi.org/10.1021/bm049593m.
[18] L. Liu, X. Tang, Y. Wang, S. Guo, Smart gelation of chitosan solution in the presence of NaHCO3 for injectable drug delivery system, Int. J. Pharm. 414 (2011) 6–15, https://doi.org/10.1016/j.ijpharm.2011.04.052.
[19] E. Assaad, M. Maire, S. Lerouge, Injectable thermosensitive chitosan hydrogels with controlled gelation kinetics and enhanced mechanical resistance, Carbohydr. Polym. 130 (2015) 87–96, https://doi.org/10.1016/j.carbpol.2015.04.063.
[20] M. Mekhail, J. Daoud, G. Almazan, M. Tabrizian, Rapid, guanosine 5'-diphosphate-induced, gelation of chitosan sponges as novel injectable scaffolds for soft tissue engineering and drug delivery applications, Adv. Healthcare Mater. 2 (2013) 1126–1130, https://doi.org/10.1002/adhm.201200371.
[21] L. Dambies, T. Vincent, A. Domard, E. Guibal, Preparation of chitosan gel beads by ionotropic molybdate gelation, Biomacromolecules 2 (2001) 1198–1205, https://doi.org/10.1021/bm010083r.
[22] D. Komoto, T. Furuike, H. Tamura, Preparation of polyelectrolyte complex gel of sodium alginate with chitosan using basic solution of chitosan, Int. J. Biol. Macromol. 126 (2019) 54–59, https://doi.org/10.1016/j.ijbiomac.2018.12.195.
[23] M. Balima, I. Morfin, G. Sudre, A. Montembault, Stretchable hydrogels of chitosan/hyaluronic acid induced by polyelectrolyte complexation around neutral pH, Carbohydr. Polym. 339 (2024) 122265, https://doi.org/10.1016/j.carbpol.2024.122265.
[24] A. Montembault, C. Viton, A. Domard, Physico-chemical studies of the gelation of chitosan in a hydroalcoholic medium, Biomaterials 26 (2005) 933–943, https://doi.org/10.1016/j.biomaterials.2004.03.033.
[25] T. Gréa, G. Jacquot, A. Durand, C. Mathieu, A. Gasser, C. Zhu, M. Banerjee, E. Hucteau, J. Mallard, P. Lopez Navarro, B.V. Popescu, E. Thomas, D. Kryza, J. Sidi-Boumedine, G. Ferrauto, E. Gianolio, G. Fleith, J. Combet, S. Brun, S. Erb, S. Cianferani, L.J. Charbonnière, L. Fellmann, C. Mirjolet, L. David, O. Tillement, F. Lux, S. Harlepp, X. Pivot, A. Detappe, Subcutaneous administration of a zwitterionic chitosan-based hydrogel for controlled spatiotemporal release of monoclonal antibodies, Advanced Materials n/a (2023) 2308738, https://doi.org/10.1002/adma.202308738.
[26] A. Hirai, H. Odani, A. Nakajima, Determination of degree of deacetylation of chitosan by 1H NMR spectroscopy, Polym. Bull. 26 (1991) 87–94, https://doi.org/10.1007/BF00299352.
[27] C. Schatz, C. Viton, T. Delair, C. Pichot, A. Domard, Typical physicochemical behaviors of chitosan in aqueous solution, Biomacromolecules 4 (2003) 641–648, https://doi.org/10.1021/bm025724c.
[28] M. Natuzzi, C. Grange, T. Gréa, T. Brichart, A. Aigle, D. Bechet, B. Hautefeuille, E. Thomas, J.-Y. Ayoub, J.-M. Bonnet, V. Louzier, B. Allaouchiche, A. Couturier, A. Montembault, P.N. de Oliveira, L. David, F. Lux, O. Tillement, Feasibility study and direct extraction of endogenous free metallic cations combining hemodialysis and chelating polymer, Sci. Rep. 11 (2021) 19948, https://doi.org/10.1038/s41598-021-99462-y.
[29] A. Durand, T. Borisova, F. Lux, J.A. Howard, A. Tillement, H. Kuznietsova, N. Dziubenko, V. Lysenko, L. David, D. Morel, R. Berbeco, S. Komisarenko, O. Tillement, E. Deutsch, Enhancing radioprotection: a chitosan-based chelating polymer is a versatile radioprotective agent for prophylactic and therapeutic interventions against radionuclide contamination, PLoS One 19 (2024) e0292414, https://doi.org/10.1371/journal.pone.0292414.
[30] J. Moreau, E. Guillon, J.-C. Pierrard, J. Rimbault, M. Port, M. Aplincourt, Complexing mechanism of the lanthanide cations Eu3+, Gd3+, and Tb3+ with 1,4,7,10-Tetrakis(carboxymethyl)-1,4,7,10-tetraazacyclododecane (dota)—characterization of three successive complexing phases: study of the thermodynamic and structural properties of the complexes by potentiometry, luminescence spectroscopy, and EXAFS, Chem. Eur J. 10 (2004) 5218–5232, https://doi.org/10.1002/chem.200400006.

[31] M. Costalat, L. David, T. Delair, Reversible controlled assembly of chitosan and dextran sulfate: a new method for nanoparticle elaboration, Carbohydr. Polym. (2014), https://doi.org/10.1016/j.carbpol.2013.10.098.
[32] T. Kim, J. Shin, B. An, Adsorption characteristics for Cu(II) and phosphate in chitosan beads under single and mixed conditions, Polymers 15 (2023) 421, https://doi.org/10.3390/polym15020421.
[33] B.V. Slaughter, S.S. Khurshid, O.Z. Fisher, A. Khademhosseini, N.A. Peppas, Hydrogels in regenerative medicine, Adv. Mater. 21 (2009) 3307–3329, https://doi.org/10.1002/adma.200802106.
[34] T. Delair, Colloidal polyelectrolyte complexes of chitosan and dextran sulfate towards versatile nanocarriers of bioactive molecules, Eur. J. Pharm. Biopharm. 78 (2011) 10–18, https://doi.org/10.1016/j.ejpb.2010.12.001.
[35] C. Pochat-Bohatier, A. Venault, D. Bouyer, L. Vachoud, L. David, C. Faur, Development and characterization of composite chitosan/active carbon hydrogels for a medical application, J. Appl. Polym. Sci. 128 (2013) 2945–2953, https://doi.org/10.1002/app.38414.
[36] A. Guinier, G. Fournet, Small-angle Scattering of X-Rays, Wiley, 1955.
[37] S. Popa-Nita, P. Alcouffe, C. Rochas, L. David, A. Domard, Continuum of structural organization from chitosan solutions to derived physical forms, Biomacromolecules 11 (2010) 6–12, https://doi.org/10.1021/bm9012138.
[38] C.J. Brinker, G.W. Scherer, Sol-gel Science : the Physics and Chemistry of Sol-Gel Processing, 2013.
[39] Y. Ogawa, P.-K. Naito, Y. Nishiyama, Hydrogen-bonding network in anhydrous chitosan from neutron crystallography and periodic density functional theory calculations, Carbohydr. Polym. 207 (2019) 211–217, https://doi.org/10.1016/j.carbpol.2018.11.042.
[40] M. Robitzer, L. David, C. Rochas, F. Di Renzo, F. Quignard, Supercritically-dried alginate aerogels retain the fibrillar structure of the hydrogels, Macromol. Symp. 273 (2008) 80–84, https://doi.org/10.1002/masy.200851311.
[41] M. Robitzer, L. David, C. Rochas, F. Di Renzo, F. Quignard, Nanostructure of calcium alginate aerogels obtained from multistep solvent exchange route, Langmuir 24 (2008) 12547–12552, https://doi.org/10.1021/la802103t.
[42] G. Kim, H. Hugonnet, K. Kim, J.-H. Lee, S.S. Lee, J. Ha, C. Lee, H. Park, K.-J. Yoon, Y. Shin, G. Csucs, I. Hitchcock, L. Mackinder, J.H. Kim, T.H. Hwang, S. Lee, P. O'Toole, B.-K. Koo, J. Guck, Y. Park, Holotomography, Nat Rev Methods Primers 4 (2024) 1–22, https://doi.org/10.1038/s43586-024-00327-1.
[43] T. Kean, M. Thanou, Biodegradation, biodistribution and toxicity of chitosan, Adv. Drug Deliv. Rev. 62 (2010) 3–11, https://doi.org/10.1016/j.addr.2009.09.004.
[44] B. Reid, M. Gibson, A. Singh, J. Taube, C. Furlong, M. Murcia, J. Elisseeff, PEG hydrogel degradation and the role of the surrounding tissue environment: PEG hydrogel degradation and the role of the surrounding tissue environment, J Tissue Eng Regen Med 9 (2015) 315–318, https://doi.org/10.1002/term.1688.
[45] T. Yu, W. Wang, S. Nassiri, T. Kwan, C. Dang, W. Liu, K.L. Spiller, Temporal and spatial distribution of macrophage phenotype markers in the foreign body response to glutaraldehyde-crosslinked gelatin hydrogels, J. Biomater. Sci. Polym. Ed. 27 (2016) 721–742, https://doi.org/10.1080/09205063.2016.1155881.